Argon/dust and pure argon pulsed plasmas explored using a spatially-averaged model

Igor Denysenko, Ilija Stefanovic, Maxime Mikikian, Eva Kovacevic, Johannes Berndt

Argon/dust and pure argon pulsed plasmas explored using a spatially-averaged model

I B Denysenko[1,2,3], I Stefanović [4], M Mikikian[2], E Kovacevic[2] and J Berndt[2]

[1]School of Physics and Technology, V N Karazin Kharkiv National University, Kharkiv, Ukraine
[2]GREMI, UMR7344 CNRS/Université d'Orléans, F-45067 Orléans, France
[3]Le Studium, Loire Valley Institute for Advanced Studies, Orléans & Tours, France
[4]Institute of Technical Sciences, Serbian Academy of Sciences & Arts, 11000, Belgrade, Serbia

E-mail: idenysenko@yahoo.com

Received
Accepted for publication
Published

Abstract

The properties (densities of electrons and metastable argon atoms, effective electron temperature and dust charge) of argon/dust and pure argon pulsed plasmas are studied using a spatially-averaged model. The calculated time-dependencies for the densities of electrons and metastable atoms are compared with the experimental measurements and are found to be in a good qualitative agreement. It is analyzed how the plasma properties depend on the shape of the electron energy probability function (EEPF), the pulsing frequency and the duty cycle for both dust-free and dusty plasma. The analysis reveals that the agreement between theory and experiment is better with Druyvesteyn EEPF than the Maxwellian EEPF. Further, the variation in the pulsing frequency ν_p differently affects the metastable density n_m in a dust-free and in a dusty plasma. For large ν_p, the metastable density in the dust-free pulsed plasma is larger than in the continuous-wave (CW) discharge, while the opposite is obtained in the presence of dust particles. This difference probably arises because of faster variation in the effective electron temperature in the dusty plasma due to collection of electrons by dust particles. Our calculations also show that dust particles may affect the behavior of electron density in the beginning of the on-period due to an enhancement in electron collection by dust particles.

Keywords: plasma, dust particles, pulsing frequency, duty cycle, spatially-averaged model

1. Introduction

Gas discharges containing charged nano and micro particles (dust particles) have been extensively studied for several decades [1 – 3] as these dusty plasmas are involved in many technological and bioimaging applications and also in fusion research [1, 4 – 6]. They are also of a fundamental interest and have attracted research attention in diverse fields, including the formation of Coulomb dust crystals, dust vortices and voids, cosmic clouds, etc. [1–3, 7, 8]

Many properties of gas discharges with dust particles have been investigated both experimentally and numerically focusing mostly to the continuous wave (CW) regime [1–3, 7–13]. However, in many technological applications, plasma systems are not stationary [14]. Nonstationary gas discharges (especially pulsed systems) are often employed for reduction of charge accumulation on the substrates, improving the quality of the deposited films and etch selectivity [14, 15], controlling particle formation in chemically active plasmas, etc. [16–18] Therefore, dust particles in nonstationary gas discharges and afterglow plasmas have also been studied by some authors [13, 19–21].

In [19], the time-dependence of the charge of micrometer dust particles in the afterglow of a RF plasma under microgravity conditions was analyzed experimentally and theoretically. It was found that dust particles keep a negative charge for a long time in the afterglow. According to [20], negatively and positively charged dust particles as well as neutral ones coexisted for more than a minute in a RF discharge afterglow. By analyzing the dust particle diffusion in the afterglow, several properties of a dusty plasma are established [21].

A symmetrically – driven RF discharge was used to analyze the pulsed dusty plasmas with large dust charge densities ($|n_d Z_d| \geq n_e$, where Z_d is the dust charge number in units of elementary charge e, n_e and n_d are the densities of electrons and dust particles, respectively) [22–25]. Dust particles were first formed in Ar/C_2H_2 plasma and then the acetylene input was stopped to keep only an argon/dusty plasma. However, acetylene could remain in the chamber from the growth phase or due to the desorption of C_2H_2 from the chamber walls. The experiments showed that the electron density increased unexpectedly at the very beginning of the dusty plasma afterglow [24, 25]. Several mechanisms were proposed to describe this phenomenon. Firstly, the increase of the electron density in the early afterglow was attributed to the release of electrons from the dust particles by secondary electron emission in ion-dust collisions [25]. The other sources of electrons in the early afterglow were identified and compared, such as electron generation in metastable-metastable and metastable-dust collisions [22] or secondary electron emission from electrodes [26]. In a presence of impurities, such as acetylene, the metastable – acetylene collisions make a significant contribution to the described phenomenon [27].

Note that in most theoretical studies of nonstationary dusty plasmas, the electron energy probability function (EEPF) was assumed to be Maxwellian, whereas, in practice, the EEPF in low-temperature plasmas is usually non-Maxwellian [28–30]. Moreover, in [22–26] the authors focused their attention mainly on the off-period (afterglow). Therefore, these studies did not provide information about the time variation of plasma properties during the on-period and about the dependence of plasma properties on the pulsing parameters (frequency ν_p, duty cycle η). Nevertheless, this information is important to control pulsed plasma properties in different technological applications [14, 16, 31].

In this paper, we propose a theoretical description for a pulsed dusty plasma with large dust charge densities. The current model formulation is based on a spatially-averaged (0D) model, which describes both the on- and off-periods of the pulsed plasma and accounts for the non-Maxwellian shape of the EEPF. Thus, this 0D model differs significantly from the models used in our previous studies of pulsed dusty plasmas, where only the afterglow is considered and the electrons are assumed to be Maxwellian [22, 26]. Beside of that, the model uses recently proposed rate constant for argon metastable – metastable collisions (known also as "metastable pooling"), and the new Penning branching ratio in Ar*- C_2H_2 reaction $\alpha = 0.3$ [27]. The metastable pooling rate is a few times lower compared to the value commonly used in the literature [32]. The model is used to study plasma properties (the electron and metastable atoms' densities, effective electron temperature and dust charge) as a function of time in pure argon and dusty pulsed discharges. It is also studied how the plasma properties depend on the shape of the EEPF, the pulsing frequency and the duty cycle. For the sake of comparison, the studies are carried out for the conditions close to those in the experiments [16, 25, 27]. The calculated time-dependencies for densities of electrons and metastable argon atoms are compared with measurements from [22, 27] for dust-free and dusty plasma.

2. Theoretical model

In the 0D model, it is assumed that the gas-discharge plasma has $R = 15$ cm radius and $L = 7$ cm height and consists of electrons with density n_e, singly charged positive ions (Ar^+) with density n_i, dust particles with density n_d, radius a_d and negative charge eZ_d, ground-state argon atoms (Ar_0) with density n_a, metastable argon atoms (Ar_m) with density n_m, argon atoms in the resonance 4s states ($^3P_1$ and $^1P_1$) (Ar_r) with density n_r as well as argon atoms in 4p states (Ar_{4p}) with density n_{4p}. The metastable and resonance atom densities n_m, n_r and n_{4p} represent the density of a composite ($^3P_0$ and $^3P_2$) metastable level, the density of a composite ($^3P_1$ and $^1P_1$) resonance level and the density of a composite 4p state, respectively. It is assumed that ions and dust particles are at gas temperature T_g and ions have Maxwellian distribution. In numerical simulations, the gas temperature T_g is considered to be 294 K and 366 K in the dust-free and dusty cases, respectively [33].

The electron energy probability function (EEPF) is described by the following expression [34]

$$F(\varepsilon) = A_1\, exp(-A_2 \varepsilon^x), \tag{1}$$

where ε is the electron energy and x takes different values according to the shape of EEPF: $x = 1$ and $x = 2$ for Maxwellian and Druyvesteyn electron energy distributions, respectively. The coefficients A_1 and A_2 are functions of x and the average electron energy [34] $\langle\varepsilon\rangle = \int_0^\infty \varepsilon\, F(\varepsilon)\sqrt{\varepsilon} d\varepsilon = \frac{3}{2} eT_{\text{eff}}$ and T_{eff} is the effective electron temperature. The EEPF has the following normalization $\int_0^\infty F(\varepsilon)\sqrt{\varepsilon} d\varepsilon = 1$.

In most of the cases considered in the next section, we will assume that the EEPF is Druyvesteyn-like. This distribution is typical for laboratory plasmas sustained by an RF generator with the frequency f =13.56 MHz at $n_e < 10^{11}$ cm^{-3} and $Pd > 0.2$ Torr×cm [35], where P is the argon gas pressure and $d \approx L/2$ is the dimension of the reactor in cm. However, effects of variation of the EEPF shape on plasma properties will be also studied.

The particle balance equation for a species X (electrons and argon atoms in excited states) is given as

$$\frac{\partial n^{(X)}}{\partial t} = \sum_i R_{G,i}^{(X)} - \sum_i R_{L,i}^{(X)}, \tag{2}$$

where $R_{G,i}^{(X)}$ and $R_{L,i}^{(X)}$ are, respectively, the rates for reactions of the various generation and loss processes of the species X. It is assumed that in both pure argon and dusty pulsed plasmas, electrons are generated in collisions of electrons with argon atoms in the ground and excited states (4p and 4s states), as well as in metastable–metastable collisions (metastable pooling). In the dusty plasma, we assume that electrons can be additionally produced in one of the two processes: secondary

electron emission in collisions of excited argon atoms Ar*(Ar_m, Ar_r and Ar_{4p}) with dust particles with the effective secondary emission yield γ_m [22] and interaction of excited atoms with acetylene molecules [27]. In the latter case, it is assumed that acetylene molecules are present in small amounts in the pulsed dusty plasma. The experimental procedure of making the dust plasma involves the use of acetylene as a precursor that could remain in the chamber from the previous phase of the experiment when the dust particles are formed in Ar/C_2H_2 plasma, or due to the desorption of C_2H_2 from the chamber walls [27]. The interaction of excited atoms with acetylene molecules is characterized by the quenching rate coefficient k_q=5.6×10^{-10} cm^{3}s^{-1} and by the Penning branching ratio in Ar*- C_2H_2 reaction α = 0.3 [27]. Here, we consider the acetylene as an impurity with the very low density (~10^{11} cm^{-3}) compared to the argon (~10^{15} cm^{-3}) in the dusty pulsed plasma. Therefore, these impurity molecules do not affect essentially the ion composition and the energy balance in the plasma volume.

The model assumes that electrons and ions are lost from the discharge because of their diffusion to the walls and by deposition on dust particles.

In the model, the ion density n_i is found from the quasineutrality condition

$$n_i - n_e + n_d Z_d = 0. \qquad (3)$$

Considering various collisional processes in the plasma volume, we account only for binary collisions. A reaction rate for such reactions is calculated as the product of the reactants' densities and the rate coefficient K of the reaction, $R = K \times n_\alpha n_\beta$, where n_α and n_β are the densities of the reactants. The electron production and loss processes are listed in the table 1.

The rate coefficients for reactions (R1)-(R4) are calculated using the corresponding reaction cross sections σ taken from [36-38] ($K = \int_0^\infty \sigma(\varepsilon)\sqrt{2e\varepsilon/m_e}\,F(\varepsilon)\sqrt{\varepsilon}d\varepsilon$, where m_e is the electron mass). In the most cases considered in our paper, the rate for metastable pooling is taken to be K_p = 1.24 ×10^{-10} cm^3/s (about 10 times smaller than in [39], as it was proposed in [27]). The calculations are also carried out for the value K_p = 6.2 ×10^{-10} cm^3/s, which is commonly used in simulation works [22, 40].

The rate for electron diffusion to the walls R_w is calculated assuming that the total ion and electron fluxes to the walls are equal, i.e. $R_W = n_i k_{wi}$, where $k_{wi} = 2u_B \frac{R^2 h_L + RLh_R}{R^2 L}$. Here, $u_B = \langle\varepsilon\rangle^{1/2}\left(\frac{2e}{m_i}\right)^{1/2}\frac{\Gamma(\xi_1)}{[\Gamma(\xi_2)\Gamma(\xi_3)]^{1/2}}$ is the Bohm velocity [34], $\Gamma(\xi)$ is the gamma function with $\xi_1 = 3/2x, \xi_2 = 5/2x$ and $\xi_3 = 1/2x$, m_i is the ion mass and h_L and h_R are the edge to centre positive ion density ratios [34]. The rate coefficient for collisions of argon atoms in excited states with dust particles is $K_m^d = \pi a_d^2\sqrt{8eT_i/\pi m_i}$. The rate coefficient for deposition of electrons on negatively charged dust particles is calculated as $K_e^d = \pi a_d^2 \int_{-\varphi_s}^\infty \left(1 + \frac{\varphi_s}{\varepsilon}\right)\sqrt{\frac{2e\varepsilon}{m_e}}F(\varepsilon)\sqrt{\varepsilon}d\varepsilon$, where $\varphi_s = \frac{eZ_d}{a_d}$ is the dust surface potential. In the case when acetylene impurity is in the plasma, we assume that Ar* - C_2H_2 collisions are accompanied by production of electrons (table 1) and by loss of Ar* atoms (table 2). Since the density of C_2H_2 molecules is assumed to be very low here, we do not consider in our model the following products of this reaction: $C_2H_2^+$, C_2H and H.

Table 1. Production and loss processes of electrons relevant for the model.

Reaction	Rate	Reference
(R1) e + Ar_0 → Ar^+ + 2e	$K^{R1} = f(F,\sigma)$	[36]
(R2) e + Ar_m → Ar^+ + 2e	$K^{R2} = f(F,\sigma)$	[37]
(R3) e + Ar_r → Ar^+ + 2e	$K^{R3} = f(F,\sigma)$	[37]
(R4) e + Ar(4p) → Ar^+ + 2e	$K^{R4} = f(F,\sigma)$	[38]
(R5) Ar_m + Ar_m → Ar + Ar^+ + e	K_p	[27, 40]
(R6) Ar_m + Ar_r → Ar + Ar^+ + e	2.1×10^{-9} cm^{3}s^{-1}	[41]
(R7) Ar(4p) + Ar(4p) → Ar^+ + Ar + e	5.0×10^{-10} cm^{3}s^{-1}	[41]
(R8) dust(Z_d) +Ar^* → dust(Z_d +γ_m) +γ_me+ Ar_0	K_m^d	[22]
(R9) e → wall	R_w	[34]
(R10) e + dust(Z_d) → dust(Z_d -1)	K_e^d	[42]
(R11) Ar^* + C_2H_2 → $C_2H_2^+$ + Ar + e	αk_q	[27]

The reactions listed in table 2, as well as the reactions (R2) –(R8) in table 1 are used to calculate the 4s resonant and 4p atoms densities.

The diffusion of metastable atoms to the walls is described by the rate D_m/Λ^2, where $D_m \approx 2.42 \times 10^{18}/n_a$ is the metastable diffusion coefficient [22, 40], n_a in cm^{-3} and $\Lambda = 1/\sqrt{(\pi/L)^2 + (2.405/R)^2}$ is the effective diffusion length.

In the afterglow, the effective electron temperature is lower than in the on-period and the energetic tail of the EEPF is depleted because of deposition of high energetic electrons on the chamber walls and dust particles [43]. Thus, we assume that in the afterglow, the rate K^{R16} is smaller (here, in 5 times) than in the on-period and the rate K^{R15} is $0.2\int_0^\infty \sigma_{15}(\varepsilon)\sqrt{2e\varepsilon/m_e}\,F(\varepsilon)\sqrt{\varepsilon}d\varepsilon$. For the on-period, the reaction rates are K^{R16} = 2×10^{-7} cm^3/s [40] and $K^{R15} = \int_0^\infty \sigma_{15}(\varepsilon)\sqrt{2e\varepsilon/m_e}\,F(\varepsilon)\sqrt{\varepsilon}d\varepsilon$, where σ_{15} is the cross section for reaction R15 according to [44].

In our model, the time evolution of the effective electron temperature is found from the power balance equation:

$$\frac{\partial}{\partial t}\left(\frac{3}{2}en_eT_{\text{eff}}\right) = \frac{(P_{\text{abs}} - P_{loss})}{V}, \qquad (4)$$

where P_{abs} is the power absorbed in the plasma volume $V = \pi R^2 L$ and $P_{\text{loss}} = P_{\text{coll}} + P_w + P_d$. Here, $P_{coll} = en_e n_a V \varepsilon_c K^{R1}$ is the power loss due to elastic and inelastic collisions of electrons with Ar atoms, ε_c is the collisional energy loss per electron-ion pair created [31] which is

calculated using the cross-sections in [36]. $P_w = en_i u_B(2\pi R^2 \square_L \varepsilon_{wL} + 2\pi RL \square_R \varepsilon_{wR})$ is the power loss due to charged particle fluxes to the walls, $\varepsilon_{wL} = \varepsilon_i + \varepsilon_e + V_{el}$ is the energy loss per charged particle for the on-period in the direction parallel to the discharge axis, $\varepsilon_{wL} = \varepsilon_i + \varepsilon_e$ is the same for the off-period when the electron energy is much smaller than the electrode bias V_{el} and electrons do not deposit on the electrodes, $\varepsilon_{wR} = \varepsilon_i + \varepsilon_e$ is the energy loss per charged particle for the direction perpendicular to the discharge axis for the both on- and off-periods. ε_i is the mean kinetic energy lost per ion [34] and ε_e is the mean kinetic energy lost per electron [34]. P_d is the power loss to the dust particles [45]. The energy loss in collisions of electrons with C_2H_2 molecules is neglected in this model because of low C_2H_2 density.

Table 2. Production and loss processes of excited argon atoms used in the model, additionally to those in table 1.

Reaction	Rate	Reference
(R12) $e + Ar_0 \rightarrow Ar_m + e$	$K^{R12} = f(F,\sigma)$	[46]
(R13) $e + Ar_0 \rightarrow Ar_r + e$	$K^{R13} = f(F,\sigma)$	[46]
(R14) $e + Ar_0 \rightarrow Ar(4p) + e$	$K^{R14} = f(F,\sigma)$	[46]
(R15) $e + Ar_m \rightarrow Ar(4p) + e$	$K^{R15} = f(F,\sigma)$	[44]
(R16) $e + Ar_m \rightarrow Ar_r + e$	K^{R16}	[40]
(R17) $e + Ar_r \rightarrow Ar_m + e$	9.1×10^{-7} cm^3s^{-1}	[41]
(R18) $e + Ar_r \rightarrow Ar(4p) + e$	$K^{R18} = f(F,\sigma)$	[44]
(R19) $e + Ar_m \rightarrow Ar_0 + e$	$K^{R19} = f(F,\sigma)$	[46, 47][a]
(R20) $e + Ar_r \rightarrow Ar_0 + e$	$K^{R20} = f(F,\sigma)$	[46, 47][a]
(R21) $e + Ar(4p) \rightarrow Ar_0 + e$	$K^{R21} = f(F,\sigma)$	[46, 47][a]
(R22) $Ar_0 + Ar_m \rightarrow Ar_0 + Ar_0$	2.1×10^{-15} cm^3s^{-1}	[41]
(R23) $Ar_r \rightarrow Ar + \hbar\omega$	10^5 s^{-1}	[41]
(R24) $Ar(4p) \rightarrow Ar + \hbar\omega$	3.2×10^7 s^{-1}	[41]
(R25) $Ar(4p) \rightarrow Ar_m + \hbar\omega$	3.0×10^7 s^{-1}	[41]
(R26) $Ar(4p) \rightarrow Ar_r + \hbar\omega$	3.0×10^7 s^{-1}	[41]
(R27) $Ar_m \rightarrow Ar_0$ (wall)	D_m / Λ^2	[22, 40]
(R28) $Ar^* + C_2H_2 \rightarrow C_2H + H + Ar + e$ or $C_2H_2 + Ar + \hbar\omega$	$(1-\alpha)k_\mathrm{q}$	[27]

[a] Obtained by applying the principle of detailed balancing to the cross section given in the cited reference.

We assume that the power is modulated by an ideal rectangular waveform

$$P_{\mathrm{abs}} = \begin{cases} P_{\max} & \text{for } (k-1)\tau \le t < (k-1)\tau + \eta\tau, \\ 0 & \text{for } (k-1)\tau + \eta\tau \le t < k\tau, \end{cases}$$

where τ is the full cycle period, η is the duty cycle, and k is a positive integer. $P_{\mathrm{abs}} = P_{\max}$ for the on-period and $P_{\mathrm{abs}} = 0$ for the off-period. The time averaged absorbed power for the full cycle $< P_{\mathrm{abs}} >$ is ηP_{max}.

Considering the afterglow phase, we additionally assume that due to the production of energetic electrons in metastable–metastable collisions, super-elastic electron–metastable collisions and emission processes, the effective electron temperature cannot be smaller than the afterglow temperature $T_{aft} \le 0.15$ eV, i.e. after its decay to reach T_{aft}, T_{eff} becomes time-independent. T_{aft} is a parameter chosen to match theoretical results and experimental data well.

The next equation of our system is the equation for the dust particle charge. The standard OML theory is usually used to describe the *equilibrium* dust charge in complex plasma. Nevertheless, several authors have shown that in the case of complex plasma OML theory fails to describe the dust charging in an appropriate way [48]. In order to describe the dust charging more accurately we (i) correct the ion current to the dust particles taking into account the ion neutral collisions [48] and (ii) include the additional processes which are relevant for dust charging [24, 25]. These processes, such as *secondary electron emission* by collisions of excited argon atoms with dust, have been neglected by OML theory. Nevertheless they play a significant role in dust charging/discharging processes under certain conditions [24, 25]. According to the assumptions (i) and (ii) the time – dependent dust charge follows the equation

$$\frac{\partial Z_d}{\partial t} = K_i^d n_i + \gamma_m K_m^d (n_m + n_r + n_{4\mathrm{p}}) - K_e^d n_e. \quad (5)$$

Here $K_i^d \approx a_d^2 \left(8\pi e T_i / m_i\right)^{0.5} \left(1 + \xi\tau + H\xi^2\tau^2 \lambda_S n_a \sigma_{ia}\right)$ is the rate for collection of ions by dust particles, which accounts for ion-neutral collisions in the sheath around a dust particle [48]. $\tau = T_{\mathrm{eff}}/T_i$, $\xi = |Z_d| e / \left(a_d T_{\mathrm{eff}}\right)$ and $\sigma_{ia} \approx 10^{-14}$ cm^2 is the cross-section for ion-neutral collisions. The function H has the following asymptotes: $H \sim 0.1$ for $0.1 \le \beta \le 10$; $H \sim \beta$ for $\beta << 1$ and $H \sim \beta^{-2} (\ln\beta)^3$ for $\beta >> 1$ [48], where $\beta = |Z_d| e / \left(\lambda_s T_i\right)$ and λ_s is the screening length, which is of the same order as the Debye length [1].

The second term in the right-hand side of equation (5) accounts for electron emission in metastable-dust collisions. This process is not considered with acetylene impurity inside the plasma. The last term in the right-hand side of equation (5) describes the electron losses to the dust. When the plasma equilibrium is established, like at the end of the on- phase, the left -hand side of (5) becomes zero. Further, if the secondary electron emission is neglected when e.g. the density of argon reactive species is low, the equation (5) simplifies to the standard form used in OML theory.

The equations for each particle (electrons, excited argon atoms in metastable and 4s and 4p resonance states), the power balance equation and the equation for dust charge are solved by using the DVODE package [49]. First, it is found a steady-state ($\frac{\partial}{\partial t} = 0$) solution of these equations corresponding to $P_{\mathrm{abs}} = P_{\max}$. Then, using this solution, the plasma parameters (n_e, n_m, n_r, $n_{4\mathrm{p}}$, - Z_d and T_{eff}) as a function of time are calculated for the case of pulsed plasma.

3. Results and discussion

Using the volume-averaged model, we have calculated plasma properties (n_e, n_m, T_{eff} and Z_d) as a function of time in dust-free and dusty plasma. The simulations have been carried out for the conditions typical to experiments on pure argon and argon/dust pulsed plasmas [22, 27], in particularly, for the same electron densities at the end of the on-period as in the experiments. The calculated time-dependencies for electron and metastable densities have been compared with the experimental values in [22, 27]. We have also analyzed how these plasma parameters depend on the EEPF shape (which is characterized by the parameter x), the pulsing frequency and the duty cycle.

3.1. Calculated time-dependencies of different plasma properties and their comparison with experimental values

In the experiments [22, 27], a 13.56 MHz capacitively-coupled plasma discharge is ignited between two parallel plate R=15 cm radius electrodes L=7 cm separated. Both electrodes are powered by an RF signal with power in the range 10 to 80 W and delivered from an RF generator through a specially designed matching box. The working gas is either pure argon or argon-acetylene mixture at a continuous flow rate of 8 sccm (argon) and 0.5 sccm (acetylene), keeping the total pressure constant at 10 Pa. The discharge is driven either in CW or in pulsed mode, with a variable pulsing frequency and a fixed duty cycle of 0.5.

To generate the dust particles, it is necessary to use the acetylene precursor, which in some particular plasma conditions initiate the dust growth. In CW mode the nanoparticles are forming spontaneously after adding the acetylene to the argon. In the pulsed regime, however, it is necessary to run the discharge for at least 3 min and at pulsing frequencies above 700 Hz in order to form the dust [27]. Interrupting the C_2H_2 flow stops the nanoparticles' growth and for the next few minutes the particles stay imprisoned in the plasma bulk even at the lower pulsing frequency, thus forming the argon-dust plasma without C_2H_2. After forming the dust, the discharge is driven with the RF signal modulated by a rectangular signal frequency of 105 Hz with 0.5 duty cycle. Electron density is measured by microwave interferometry [16], while metastable density is deduced using laser absorption spectroscopy [27, 50]. Both measurements give values integrated over the plasma length.

3.1.1. Dust-free pulsed plasma

Figure 1 illustrates the temporal behavior of the line-of-sight averaged electron density (*a*) and Ar* $1s_5$ metastable density (*b*) measured at the mid-plane between electrodes and the corresponding simulation results. Numerical results are obtained for V_{el} =58.0 V [51], K_p = 1.24 ×10^{-10} cm^3/s, T_{aft} = 0.15 eV, T_g = 294 K and x=2. Note that figure 1 shows cycles taken in a middle of a long sequence, so before 0 s it is the end of another cycle. For both species, good quantitative agreement exists between the calculated and experimental time-dependencies. However, the agreement is better for the afterglow phase than for the on-period where the model gives a faster increase at the beginning of the on-period. In addition, there is a maximum in the calculated n_m at the beginning of the on-period that is not observed in the experiment.

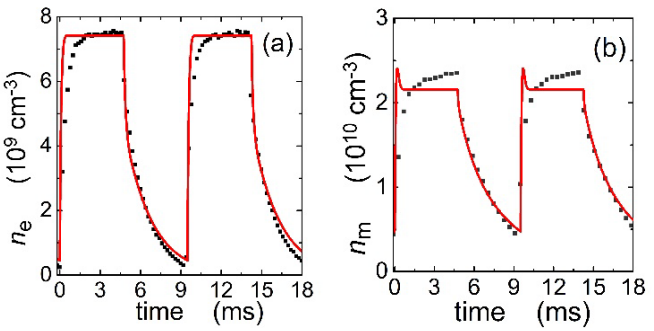

Figure 1. Electron (*a*) and metastable (*b*) densities as a function of time in a pure argon pulsed plasma. Solid lines — model; black squares — experiment [22, 27, 33]. Zero time indicates the beginning of the on-period. The off-period (afterglow phase) starts at 4.75 ms and ends at 9.5 ms.

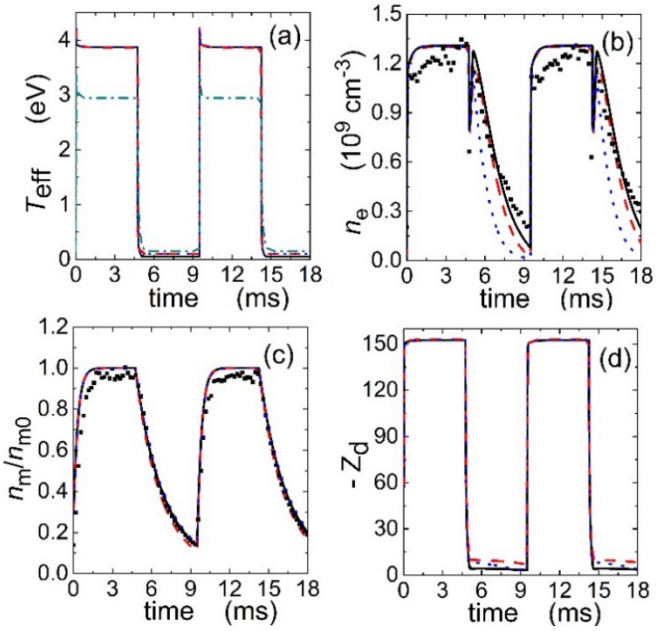

Figure 2. T_{eff} (*a*), n_e (*b*), n_m/n_{m0} (*c*) and -Z_d (*d*) in an argon/dust pulsed plasma. (i) The solid and dotted curves are calculated taking into account secondary electrons in metastable-dust collisions with n_{m0}=9.82×10^{10} cm^{-3}, T_{aft} = 0.05 eV or T_{aft} = 0.1 eV for the solid and dotted curves, respectively; (ii) dashed curves – electrons are generated in collisions of metastable atoms with acetylene molecules with n_{m0}=9.64×10^{10} cm^{-3} and T_{aft} = 0.1 eV. For the comparison, the dash-dotted curve in figure (*a*) represents T_{eff} in a pure argon pulsed plasma. The black squares in figures (*b*) and (*c*) are experimental data from [22, 27]. n_{m0}=1.75×10^{11} cm^{-3} is a measured value reported in [22, 27].

During the on-period, n_m depends on n_e and T_{eff} strongly, because the formation of metastable atoms occurs mainly in collisions of electrons with argon atoms in the ground state. During the initial stage of the on-period, a sharp spike in T_{eff} is observed (figure 2(*a*)). This is due to a small number of electrons left in the discharge at the end of the previous afterglow phase. At the beginning of the new on-period, the RF power is absorbed by this small number of electrons inducing their strong heating and thus a higher T_{eff} explaining also the sharp spike in n_m. Note that spikes in the electron temperature and density of excited species at the very beginning of the on-period are observed in a few numerical and experimental studies on pulsed plasmas in various reactor geometries and plasma conditions [52 - 54].

In the afterglow phase, n_e and n_m monotonically decrease mainly due to diffusion to the chamber walls [22]. Nevertheless, the loss of metastable atoms in collisions with electrons prevails in the early afterglow [22].

3.1.2. Dusty plasma

The presence of dust in plasma introduces additional production and loss processes for electrons and Ar metastables. Two additional processes are analyzed separately in two different scenarios: (i) secondary electrons are generated by metastable–dust collisions; (ii) production of electrons by collisions of metastable atoms with acetylene impurity remaining in the plasma from the dust formation stage [27]. In the case (i), we use $\gamma_m = 0.2$ and two different afterglow temperatures T_{aft} (0.05 eV and 0.1 eV). In the case (ii), T_{aft} is 0.1 eV and the acetylene density n_{C2H2} is 10^{11} cm^{-3}, according to the figure 11(a) in [27]. In both cases, we assume that $a_d = 50$ nm, $n_d = 3.0 \times 10^7$ cm^{-3}, $T_g = 366$ K [22], $K_p = 1.24 \times 10^{-10}$ cm^3/s, V_{el} =34.0 V [51] and x=2.

The calculated n_e and n_m follow relatively well the experimental values in the case (ii) and the case (i) with T_{aft} = 0.05 eV. However, in the late afterglow, the decay time for electron density in the case (ii) is slightly shorter than in the case (i) with T_{aft} = 0.05 eV (figure 2(*b*)). This is due to larger T_{aft} and, as a consequence, larger loss of electrons due to diffusion to the walls in the former case. At larger T_{aft}, the electron flux to dust particles enhances, increasing the absolute value of dust charge number $|Z_d|$. Therefore, $|Z_d|$ in late the afterglow in the case (i) and T_{aft} = 0.05 eV is smaller than in the case (ii) (figure 2(*d*)). In addition, the secondary electron emission in metastable -dust collisions is stronger in the case (i), which reduces the negative charge on dust particles in comparison with case (ii). If T_{aft} is the same in both cases (i) and (ii), the loss of electrons on dust particles in the afterglow is larger in the case (i) because of smaller $|Z_d|$ (figure 2(*d*)) due to secondary emission. Because of larger electron loss on dust particles, in the off-period n_e drops faster in the case (i) than in the case (ii) for the same T_{aft} (figure 2(*b*)). In both cases (i) and (ii), the calculated metastable densities are nearly 1.8 times smaller than the densities measured in the experiment. This difference may be explained by simplifications introduced in the model, which will be discussed later.

Insertion of dust particles into a plasma during the on-period is accompanied by a decrease in the electron density (figures 2(*b*) and 1(*a*)) and an increase in the effective electron temperature (figure 2(a)) and the density of metastable argon atoms (figures 2(*c*) and 1(*b*)). Due to the loss of electrons and metastable atoms on dust particles, the calculated electron and metastable densities increase more slowly at the very beginning of the on-period in the presence of dust particles compared to the dust-free case (figures 1 and 2).

In the on-period, the density of ions ($n_i = n_e + n_d|Z_d|$) in the dusty plasma is smaller than $n_i (= n_e)$ in the dust-free case (figures 1(*a*) and 3). This decrease in the ion density in the dusty plasma, comparing with the dust-free plasma, is due to the decrease of electron density. In the beginning of the off-period, the density of ions in the dusty plasma drops faster than n_e in the dust-free and dusty plasma. The significant number of Ar^+ ions is captured by negatively charged dust particles, which causes this fast ion decay. The term $K_i^d n_i$ in equation (5) can be essentially larger than the term $K_e^d n_e$ (see figure 4(*b*) of [22]) because the rate K_e^d depends strongly on T_{eff} (for example, if the Maxwellian is assumed this dependence is nearly exponential), while the rate K_i^d depends weakly of the effective electron temperature. The rate K_i^d decreases with decreasing $|Z_d|$ and, therefore, for most of the off-period, when $|Z_d|$ is small (figure 2(*d*)), the decay time for n_i is nearly the same as that for n_e in the late afterglow (figures 2(*b*) and 3).

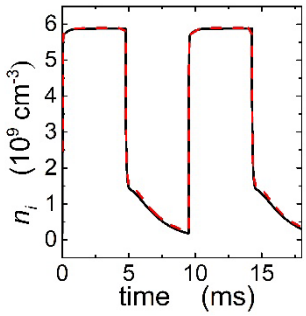

Figure 3. n_i as a function of time. The solid and dashed curves are obtained for the same conditions as the solid and dashed curves in figure 2(*b*), respectively.

In the on-period, the production of electrons occurs mainly due to electron-atom collisions, while this production process can be neglected in the afterglow. In the off-period, the main processes of electron generation are collisions of metastable atoms with other species (acetylene molecules or dust particles). In the beginning of the afterglow phase, when the metastable density is high enough, the electron production in metastable collisions is dominating the loss of electrons on the walls and dust particles, which causes a peak of n_e in the afterglow (at t~ 5.2 ms in figure 2(*b*)) [22, 27].

3.2. Effects of variation in the EEPF shape

Next, we analyze how a variation in the EEPF shape affects the plasma properties. For that, we vary the parameter

x in equation (1), while other process parameters, including n_e at the end of the on-period (at t = 4.75 ms in figure 4(a)), remain fixed.

3.2.1. Dust-free pulsed plasma

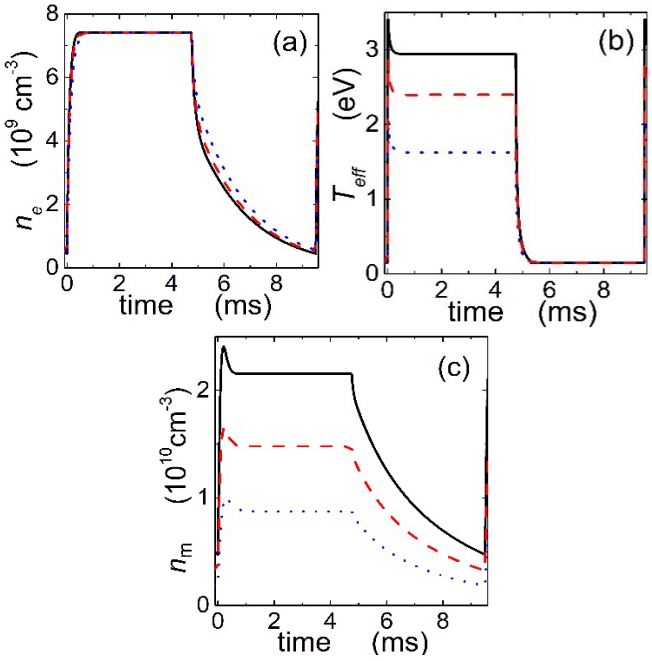

Figure 4. Calculated n_e (a), T_{eff} (b) and n_m (c) as functions of time in a pure argon pulsed plasma for different shapes of the EEPF: Solid line – x = 2, dashed line – x = 1.5 and dotted line – x = 1.

In figure 4, the time-dependencies for n_e, T_{eff} and n_m are shown for different x in the case of pure argon plasma. The external conditions and assumptions are the same as in figure 1. One can see in figure 4(b) that T_{eff} in the on-period becomes higher with increasing x because the electron energy probability function becomes more convex [55]. Due to the temperature increase, the densities of excited argon atoms, including metastables, increase too (figure 4(c)). Meanwhile, the density of electrons in the afterglow becomes smaller with increasing x (figure 4(a)) due to an enhancement of the electron loss on the walls because of the increase of the Bohm velocity. In particular, $u_B = \sqrt{eT_{eff}/m_i}$ and $u_B = \sqrt{3 \times 0.457 eT_{eff}/m_i}$ [55] for x =1 and x = 2, respectively. Here, at the beginning of the afterglow, T_{eff} (x=2) > T_{eff} (x=1), while these temperatures are equal to each other for large afterglow times.

For the case x=1, the calculated metastable density during most of the on-period is essentially smaller than that obtained in the experiment (figures 1(b) and 4(c)). According to the model the Druyvesteyn EEPF leads to the better agreement between calculated and measured values of $n_m(t)$ than Maxwellian EEPF.

3.2.2. Dusty pulsed plasma

In figure 5, T_{eff}, n_m and n_e as functions of time are shown for the case of dusty plasma and different x. The input parameters are $n_e(t$=4.75 ms)=1.3×10^9 cm^{-3}, n_{C2H2}= 10^{11} cm^{-3} and T_{aft} = 0.1 eV, and the production of electrons by electron-atom, metastable-metastable and metastable–acetylene collisions is assumed. Other parameters and assumptions, are the same as in figure 2.

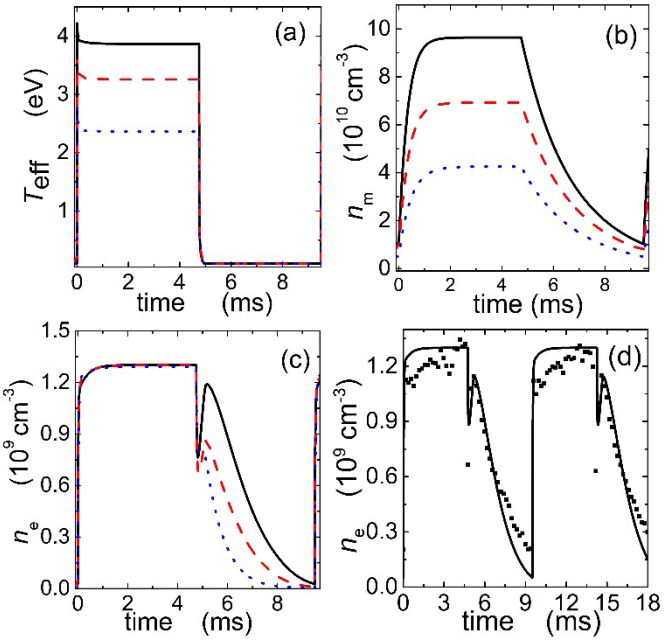

Figure 5. T_{eff} (a), n_m (b) and n_e (c) for different x: 2 (solid line), 1.5 (dashed line) and 1.0 (dotted line). (d) n_e calculated (solid line) for x=1, K_p =6.2×10^{-10} cm^3/s, T_{aft} = 0.05 eV, n_{C2H2} =10^{11} cm^{-3} and the same other conditions as in figure 2. The black squares in figure (d) are experimental data from [22, 27].

As in the case of the Druyvesteyn EEPF (figures 1 and 2), the density of metastable atoms and the effective electron temperature during the on-period are higher in a pulsed dusty plasma than in a dust-free plasma (figures 4 and 5) for the same x (=1 or 1.5). As in the case of dust-free pulsed plasma, n_m and T_{eff} increase when x becomes larger (figures 5(a) and 5(b)). The increase of n_m with x is accompanied by an enhancement of electron production in metastable-metastable collisions and collisions of metastable atoms with C_2H_2 molecules and, as a result, the electron density in the off-period increases also (figure 5(c)).

Note that the time-dependence for n_e in the case x = 1 (figure 5(c)), differs essentially from the experimental data (figure 2(b)). Moreover, at the end of the on-period, the calculated metastable densities for x=1 and x=1.5 (figure 5(b)) are much smaller than the measured one (1.75×10^{11} cm^{-3}).

The time-dependence for n_e calculated in the case x = 1 may agree well with the experimental data if one assumes that the metastable pooling process is stronger. Figure 5(d) compares the experimental data and the model results for the

$x = 1$ and $K_p = 6.2\times10^{-10}$ cm^3/s instead of 1.24×10^{-10} cm^3/s. ($K_p = 6.2\times10^{-10}$ cm^3/s is commonly used in the literature [22, 32].) Although the overall agreement is better, the stronger metastable pooling leads to much shorter electron decay time in the afterglow than expected, since $n_e \sim n_m^2$. Recent analysis [27] suggests the metastable pooling rate by order of magnitude smaller than the rate commonly used in the literature [22, 32]. In this way, by using new smaller pooling rate and Druyvesteyn EEPF the properties of argon/dust pulsed plasma are described in better agreement with the experiment.

3.3. Effects of variation in the pulsing frequency

Properties of pulsed plasmas also depend on the pulsing frequency $\nu_p = 1/\tau$ [52, 53]. Therefore, we analyze how a variation in the pulsing frequency affects plasma properties.

3.3.1. Dust-free plasma

First consider the case of dust-free plasma. In figure 6, the electron and metastable densities and effective electron temperature as functions of time in a dust-free pulsed plasma are shown for different pulsing frequencies: 210, 840, 1680 and 6720 Hz.

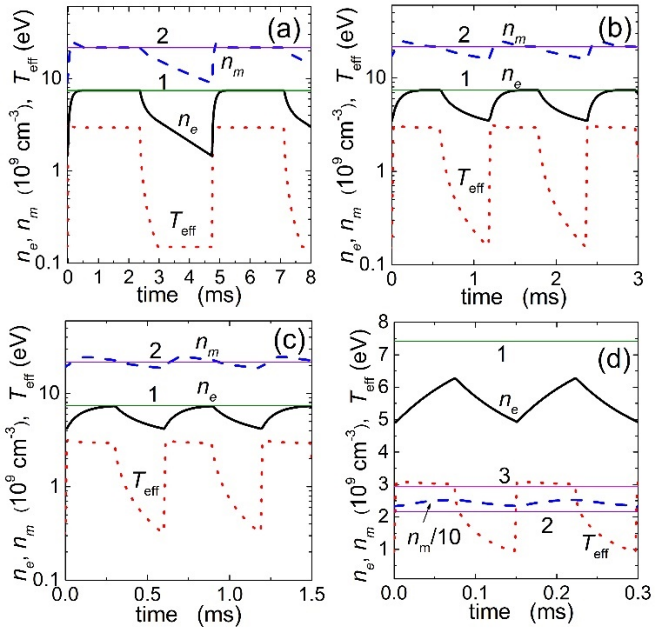

Figure 6. n_e (solid line), n_m (dashed line) and T_{eff} (dotted line) for the dust-free plasma and the different pulsing frequencies: 210 (*a*), 840 (*b*), 1680 (*c*) and 6720 (*d*) Hz. The other conditions are the same as in figure 1. The lines 1 and 2 correspond, respectively, to n_e and n_m (n_m/10 for figure 6(*d*)) calculated for the CW discharge with $P_{abs} = P_{max}$, where P_{max} = 8.7 W. The line 3 in figure 6(*d*) corresponds to T_{eff} in the CW case.

It can be seen from figure 6 that n_e during the on-period can become equal to the density in the CW discharge, in which $P_{abs} = P_{max}$, if the pulsing frequency is not high (here, $\nu_p \leq$ 1680 Hz). For large ν_p values (for example, 6720 Hz), the maximum electron density during the on-period is less than n_e in the CW discharge due to short duration of the on-period (figure 6(*d*)). The maximum effective temperature in the on-period of the pulsed plasmas is also higher than the temperature corresponding to the CW mode (T_{eff} is nearly 2.95 eV). With an increase in the pulsing frequency, the minimum values of n_e, n_m and T_{eff} (if the minimum temperature is larger than 0.15 eV) become larger because of decreasing the off-time (figure 6). Since at large values of ν_p the effective temperature during most on-time is higher than that in the CW discharge, the metastable density during the full cycle in the pulsed plasma is larger than n_m in the CW case (figure 6(*d*)).

3.3.2. Dusty plasma

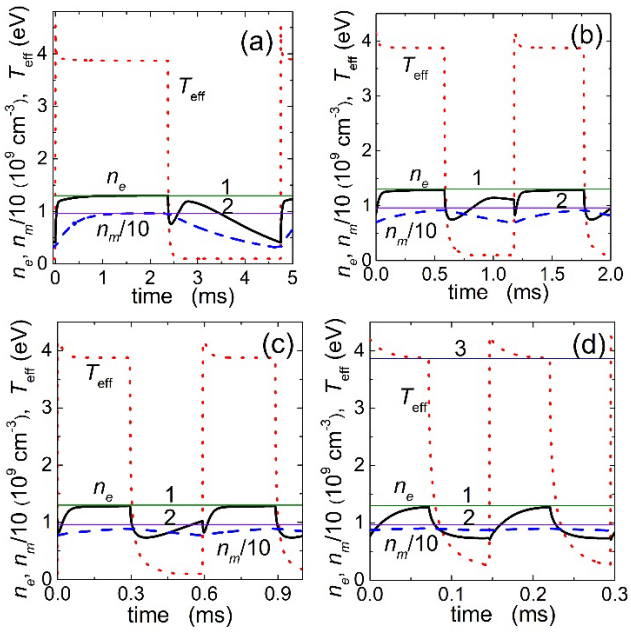

Figure 7. n_e (solid line), n_m/10 (dashed line) and T_{eff} (dotted line) as a function of time in Ar/dust pulsed plasma at different ν_p: 210 (*a*), 840 (*b*), 1680 (*c*) and 6720 (*d*) Hz. The line 1 describes n_e, the line 2 describes n_m/10 and the line 3 (only in (*d*)) T_{eff} for the CW plasma with $P_{abs} = P_{max}$. Here, P_{max} = 12.6 W and the other conditions are the same as in figure 2.

Next consider how a variation of the pulsing frequency affects the properties of an argon pulsed plasma if the plasma contains dust particles. In figure 7, the calculated time-dependencies for n_e, n_m and T_{eff} are shown for different ν_p. Again, it is assumed that electrons are produced in electron-atom, metastable-metastable and metastable-acetylene collisions. According to figure 7, if the pulsing frequency is low (for all the cases in figure 7, except for the ν_p 6.72 kHz) and $P_{abs} = P_{max}$ the electron densities in pulsed and CW plasma are equal for the most of the on-period, like in the dust-free plasma.

Note that for high pulsing frequencies, the metastable density in the pulsed dusty plasma during the full cycle is smaller than in the CW dusty plasma (figures 7(*c*) and 7(*d*)). This is opposite to the dust-free plasma, where n_m in a pulsed plasma with large ν_p is higher than the CW metastable density (figure 6(*d*)). Since in both the dust and dust-free pulsed plasmas with high ν_p the electron density for the most of the on-period is smaller than the electron density in the CW plasma, the difference in n_m, in our opinion, is due to a difference in T_{eff}. Indeed, T_{eff} in the pulsed dusty plasma varies faster than in the dust-free plasma because of the electron energy loss on dust particles [22].

At high pulsing frequencies (for example, at 6720 Hz), T_{eff} in the second half of the on-period is nearly the same as that in the CW dusty plasma (figure 7(*d*)). In the case of pure argon plasma, the effective temperature varies more slowly during the on-period, and at large ν_p, T_{eff} during most of the on-period is higher than the temperature of the CW discharge (figure 6(*d*)). Moreover, for the same high pulsing frequencies, T_{eff} in the off-period decreases more rapidly and to lower values, if dust particles are in the plasma. Therefore, the production of metastable atoms in electron-atom collisions in the afterglow lasts longer in the dust-free plasma.

There is another difference between pulsed dust-free and dusty plasmas. At some ν_p, the electron density decreases rapidly in the very beginning of the on-period in the dusty case (figures 7(*b*) and 7(*c*)). In our opinion, the increase of T_{eff} at the beginning of the on-period leads to the higher electron flux to the dust particles and the rapid decrease of n_e (figure 8(*a*)).

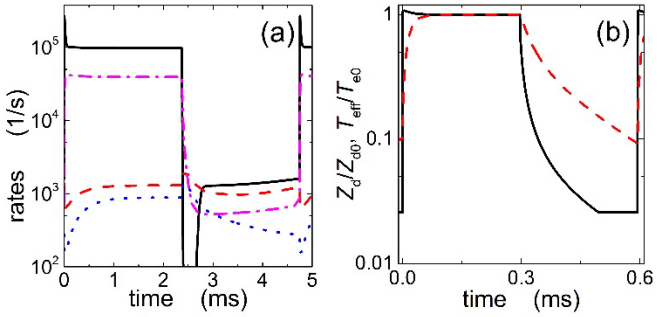

Figure 8. (*a*) The rates $K_e^d n_d$ (solid line), $n_i k_{wi}/n_e$ (dash-dotted line), $\alpha k_q(n_m+n_r+n_{4p})n_{C2H2}/n_e$ (dashed line) and $K_p n_m^2/n_e$ (dotted line) as functions of time for the 210 Hz pulsed dusty plasma. (*b*) The normalized dust charge (dashed line) and the normalized effective electron temperature (solid line) for the 1680 Hz pulsed dusty plasma. Here, Z_{d0} = - 152.64 and T_{e0} = 3.88 eV, and the other external conditions are the same as in figure 7.

Our calculations show that the rapid decrease of n_e in the beginning of the on-period is not observed at low ν_p (figure 7(*a*)), and the decrease is small for high ν_p (figure 7(*d*)). We do not observe the decrease of n_e at low ν_p because of small electron density at the end of the off-period. At smaller n_e in the end of the afterglow phase, the overshoot in T_{eff} in the beginning of the on-period is sharper [52]. As a consequence, at low ν_p, production of electrons due to ionization grows very rapidly when the power is turned on, and the production dominates the total electron loss at the beginning of the on-period. For the 6720 Hz, the decrease of electron density is smaller compared with the 840 Hz and 1680 Hz (figure 7) because of smaller rate $K_e^d n_d$ at the end of the off-period, and, consequently, smaller electron losses in the very beginning of the on-period. ($K_e^d n_d$= 0.7, 145.8 and 1282.8 s^{-1} at the end of the off-period for the frequencies 6720, 1680 and 840 Hz, respectively). For large ν_p ($\geq$ 1680 Hz), the loss of electrons on the walls described by the rate $n_i k_{wi}/n_e$ and the electron production in collisions of excited atoms with acetylene molecules (described be the rate $\alpha k_q(n_m+n_r+n_{4p})n_{C2H2}/n_e$) and in metastable-metastable collisions (described by the rate $K_p n_m^2/n_e$) are more intensive than the loss of electrons on the dust particles during the most of the off-period (figure 8(*a*)).

The rate $K_e^d n_d$ decreases rapidly in the beginning of the off-period due to the decrease of the effective electron temperature, which drops faster than $|Z_d|$ (figure 8(*b*)). The decrease of $K_e^d n_d$ in the beginning of the off-period takes place until T_{eff} reaches the afterglow temperature T_{aft}. After that, the loss rate characterizing electron deposition on dust particles increases with time, since the amount of negative charge on dust particles decreases (figure 8).

3.4. Effects of variation in duty ratio on the plasma properties

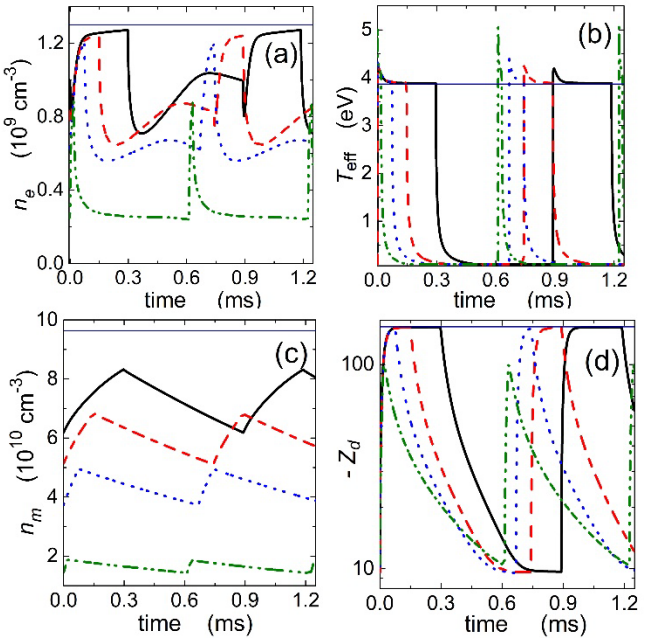

Figure 9. n_e (*a*), T_{eff} (b), n_m (*c*) and -Z_d (*d*) as a function of time in argon/dust pulsed plasma for different duty cycles: 1/3 (solid line), 1/5 (dashed line), 1/9 (dotted line) and 1/33 (dash-dot-dotted line). The duration of the off-period is 19/32 ms. The horizontal lines are for the CW mode with $P_{abs} = P_{max}$. The other external conditions are the same as for figure 7.

In figure 9, the time-dependencies for n_e (figure 9(*a*)), T_{eff} (figure 9(*b*)), n_m (figure 9(*c*)) and -Z_d (figure 9(*d*)) are shown

for the argon dusty plasma and different duty cycles: 1/3, 1/5, 1/9 and 1/33. For the sake of comparison, the same time-dependencies are also presented in figure 9 for the CW mode.

One can see from figure 9(*a*) that the maximum electron density decreases with decreasing η (figure 9(*a*)). The decrease of the maximum electron density is accompanied by a decrease of n_e at the end of the afterglow stage. Since with decreasing η, the input RF power in the beginning of the on-period is absorbed by a more limited number of electrons (smaller n_e), the overshoot in T_{eff} becomes sharper (figure 9(*b*)). Due to the decrease of n_e, the metastable density becomes smaller when η decreases (figure 9(*c*)).

With decreasing the duty cycle, the rapid decrease of n_e at the beginning of the on-period becomes less pronounced and is not observed at small η (for example, for the η = 1/33 in figure 9(*a*)). In our opinion, this is due to more rapid increase of T_{eff} at the beginning of the on-period. Indeed, since the effective electron temperature increases more rapidly with a decrease of η, the ionization rate for the production of electrons in electron-atom collisions also grows faster and, as a result, for small η the electron production dominates the total electron loss at the beginning of the on-period.

For small η, the amount of negative charges on dust particles at the end of the on-period decreases when the on-period becomes shorter (figure 9(*d*)). This is due to the decrease of the maximum electron density (figure 9(*a*)). The decrease of η is followed by the decrease of ion density too (the electron and ion densities are connected through the quasi -neutrality condition (3)). Moreover, for the small duty cycles the decay time of $|Z_d|$ in the afterglow phase is longer than for large η (figure 9(*d*)). The decrease of ion density leads to the lower ion flux to the dust and the slower discharging of the dust particles for the smaller η.

We also studied how properties of a dust-free pulsed plasma depend on the duty cycle (the results are not shown here). It was found that, similarly to the dusty plasma, for small η the electron and metastable densities in the beginning of the off-period and n_e at the end of the afterglow become smaller with decreasing the duty cycle. With a decrease of η, the overshoot in T_{eff} also becomes sharper.

4. Summary

In summary, we have developed a spatially-averaged model for an argon/dust pulsed plasma. Using the model, it has been shown how the plasma properties depend on the shape of electron energy probability function, the pulsing frequency and the duty cycle. The properties of a pure argon pulsed plasma have been also analyzed. The studies have been carried out for the external conditions close to the experimental conditions in [22, 27]. The calculated time-dependencies for electron and metastable atom densities have been compared with those obtained experimentally for dust-free and dusty plasma and found to be in a good qualitative agreement (figures 1 and 2).

In particular, it has been shown that for the same n_e at the end of the on-period, the effective electron temperature is higher and, as a result, the metastable atom density is larger in the case of Druyvesteyn EEPF (x=2) than in the Maxwellian case (x=1). This is the case for both dust-free and dusty plasmas (figures 4 and 5). However, with increasing x, the electron density in the late afterglow decreases in the dust-free plasma (figure 4(*a*)), while it becomes larger in the dusty plasma (figure 5(*c*)). This decrease in the dust-free plasma is mainly due to an increase of the electron flux to the walls (because of increasing the Bohm velocity). The increase of n_e with x in the afterglow dusty plasma is due to an enhancement of production of electrons in collisions of metastable atoms with other species (as n_m grows with x) such as acetylene molecules remaining in the plasma from the dust formation stage. For both $n_d = 0$ and $n_d \neq 0$, the calculated metastable densities agree better in magnitude with the measured n_m for the Druyvesteyn than in the Maxwellian EEPF. The new proposed argon metastable pooling rate and the new Penning branching ratio for Ar*- C_2H_2 quenching [27] supports this finding.

The pulsed plasma properties depend on the pulsing frequency. The metastable density in a dust-free pulsed plasma with high ν_p is larger than in the CW plasma for the same P_{abs} and P_{max} powers (figure 6(*d*)). This is opposite to the dusty plasma, where n_m at high ν_p is smaller than the metastable density in the CW mode (figure 7(*d*)). As the effective electron temperature variates faster the collection of electrons by dust particles becomes larger and the n_m smaller [22]. Our calculations have also shown that the electron density in a pulsed dusty plasma may decrease rapidly at the beginning of the on-period because of the rapid enhancement of collection of electrons by dust particles (figures 7(*b*) and 7(*c*)).

The properties of pulsed dusty plasma also depend essentially on the duty cycle η. The electron densities at the very beginning and at the end of the off-period decrease with a decrease of η (figure 9(*a*)). With decreasing n_e at the end of the off-period, the effective electron temperature increases more rapidly in the beginning of the next on-period (figure 9(*b*)). The rapid increase of T_{eff} is accompanied by an enhanced production of electrons (in electron-atom collisions). This larger electron production dominates the total electron loss at small η resulting in the disappearance of the rapid decrease of n_e at the beginning of the on-period (for example, for η=1/33 in figure 9(*a*)). The rapid decrease in n_e is also absent when the off-period is long (figures 2(*b*) and 7(*a*)). In our opinion, this is due to the low electron density at the end of the afterglow phase.

Note that the results of modelling enable only the qualitative analysis of argon/dust pulsed plasmas. There are some quantitative discrepancies between the results obtained from the model and the experimental data (figures 1 and 2). that can be attributed to some simplifications in the model.

In particular, the 0D model does not account for the plasma nonuniformity. Dusty plasmas are inhomogeneous and not isotropic, especially in the presence of self-organized structures, such as dust voids [2, 56]. Another difference between the model and the experiment is that the model describes the electron and metastable densities averaged over the entire plasma volume, while n_e and n_m in the experiment

are the line-of-sight averaged densities measured at the mid-plane between the electrodes [27].

Further, to calculate the dust charge the ionization in the vicinity of a dust grain is neglected. If the ionization is important [57], the expression for the rate describing collection of ions by dust particles should be taken in the more complicate form $K_i^d \approx a_d^2 \left(8\pi e T_i/m_i\right)^{0.5} \left(1+\xi\tau + H\xi^2\tau^2\lambda_S n_a \sigma_{ia}(1+\kappa)\right)$ [57], where $\kappa = n_a K^{R1}/\nu_{in}$, $\nu_{in} = \sqrt{eT_i/m_i}/\lambda_{in}$ and $\lambda_{in} = 1/n_a\sigma_{ia}$ is the ion mean-free path. Nevertheless, our calculations show that this effect does not change the dust charge and other plasma parameters significantly. This conclusion is not in contradiction with the results in [57]. In fact the results in [57] are obtained for the Maxwellian EEPF, while our results are calculated for the Druyvesteyn distribution. For the same T_{eff} Druyvesteyn distribution has fewer electrons at high energies, which results in lower ionization rate. If we use the Maxwellian distribution (figure 5), $T_{\text{eff}} \leq 2.5$ eV and the ionization events also affect the dust charge insignificantly, what is in good agreement with the results on figure 1 in [57].

In our model, we assume that a small amount of acetylene may be present in the argon/dust plasma [27]. Due to the specific formation of the carbonacous dust particles in Ar/C_2H_2 plasma the presence of small amount of impurities is inevitable [22, 27, 33]. However, the density of these impurities in the experiment is unknown at present. (To compare to the experiment the C_2H_2 density is assumed the same as in [27]). Therefore, to improve the model of the argon/dust pulsed plasma, one needs more experimental data on the plasma composition. Note also that the model does not consider the growth of dust particles. Therefore, the main task in the future will be to extend this model to describe the formation and growth of hydrocarbon grains in Ar/C_2H_2 pulsed plasma.

To summarize, this study is only a first step on the way to self-consistent modelling of dusty pulsed plasmas with large dust densities. A complete approach should include the effects of the spatial nonuniformity and the ionization events on dust charge. We expect that including these effects in the model will give the time-dependencies for n_e and n_m which will be in better qualitative agreement with experimental data than those obtained using this 0D model. Nevertheless, the model considers the main processes occurring in an argon/dust pulsed plasma, and the results from the model are in a good qualitative agreement with available experimental data. The results on dusty pulsed plasmas here are relevant to many applications involving nonstationary plasmas containing impurities, especially gas discharge plasmas used for synthesis of novel nanomaterials.

Acknowledgements

J B and E K would like to acknowledge the support from French Research Agency via ANR project PLASMABOND. I S is supported by Ministry of Education, Science and Technological Development of the Republic of Serbia according to the contract between the Institute of Technical Sciences and the Ministry No. 451-03-68/2020-14/200175.

References

[1] Bouchoule A (ed) 1999 *Dusty Plasmas: Physics, Chemistry, and Technological Impacts in Plasma Processing* (New York: Wiley)
[2] Vladimirov S V and Ostrikov K 2004 *Phys. Rep.* **393** 175
[3] Fortov V E, Ivlev A V, Khrapak S A, Khrapak A G and Morfill G E 2005 *Phys. Rep*. **421** 1
[4] Levchenko I, Keidar M, Cvelbar U, Mariotti D, Mai-Prochnow A, Fang J and Ostrikov K 2016 *J. Phys. D: Appl. Phys*. **49** 273001
[5] Kersten H, Deutsch H, Stoffels E, Stoffels W W, Kroesen G M W and Hippler R 2001 *Contrib. Plasma Phys.* **41** 598
[6] Winter J. 2000 *Phys. Plasmas* **7** 3862
[7] Arp O, Block D and Piel A 2004 *Phys. Rev. Lett*. **93** 165004
[8] Mikikian M and Boufendi L 2004 *Phys. Plasmas* **11** 3733
[9] Thomas H, Morfill G E, Demmel V, Goree J, Feuerbacher B and Möhlmann D 1994 *Phys. Rev. Lett.***73** 652
[10] Le Picard R, Markosyan A H, Porter D H, Girshick S L and Kushner M J 2016 *Plasma Chem. Plasma Process*. **36** 941
[11] Denysenko I, Berndt J, Kovacevic E, Stefanovic I, Selenin V and Winter J 2006 *Phys. of Plasmas* **13** 073507
[12] Denysenko I B *et al* 2019 *Plasma Phys. Control. Fusion* **61** 014014
[13] Denysenko I B *et al* 2020 *J. Phys. D: Appl. Phys.* **53** 135203
[14] Economou D J 2014 *J. Phys. D: Appl. Phys.* **47** 303001
[15] Samukawa S and Mieno T 1996 *Plasma Sources Sci. Technol.* **5** 132
[16] Berndt J, Kovačević E, Stefanović I and Boufendi L 2009 *J. Appl. Phys.* **106** 063309
[17] Hundt M, Sadler P, Levchenko I, Wolter M, Kersten H and Ostrikov K 2011 *J. Appl. Phys.***109** 123305
[18] Bouchoule A, Plain A, Boufendi L, Blondeau J Ph and Laure C 1991 *J. Appl. Phys*. **70** 1991
[19] Ivlev A *et al* 2003 *Phys. Rev. Lett.* **90** 055003
[20] Couëdel L, Samarian A A, Mikikian M and Boufendi L 2008 *Phys. Plasmas* **15** 063705
[21] Childs M A and Gallagher A 2000 *J. Appl. Phys*. **87** 1086
[22] Denysenko I, Stefanović I, Sikimić B, Winter J, Azarenkov N A and Sadeghi N 2011 *J. Phys. D: Appl. Phys.* **44** 205204
[23] Denysenko I B, Stefanović I, Sikimić B, Winter J and Azarenkov N A 2013 *Phys. Rev. E* **88** 023104
[24] Berndt J, Kovacević E, Selenin V, Stefanović I and Winter J 2006 *Plasma Sources Sci. Technol.* **15** 18
[25] Stefanović I *et al* 2006 *Phys. Rev. E* **74** 026406
[26] Denysenko I B, Stefanović I, Azarenkov N A and Burmaka G P 2015 *Phys. Plasmas* **22** 023702
[27] Stefanović I, Sadeghi N, Winter J and Sikimić B 2017 *Plasma Sources Sci. Technol*. **26** 065014
[28] Kolobov V I and Godyak V A 1995 *IEEE Trans. Plasma Sci.* **23** 503
[29] Kortshagen U, Busch C and Tsendin L D 1996 *Plasma Sources Sci. Technol*. **5** 1
[30] Kaganovich I D and Tsendin L D 1992 *IEEE Trans. Plasma Sci.* **20** 66
[31] Lieberman M A and Lichtenberg M A 2005 *Principle of Plasma Discharges and Material Processing*, 2 nd ed. (New Jersey: JohnWiley & Sons Inc)

[32] Ferreira C M, Loureiro J and Ricard A 1985 *J. Appl. Phys.* **57** 82
[33] Stefanović I, Sadeghi N and Winter J 2010 *J. Phys. D: Appl. Phys.* **43** 152003
[34] Thorsteinsson E G and Gudmundsson J T 2009 *Plasma Sources Sci. Technol*. **18** 045001
[35] Godyak V A, Piejak R B and Alexandrovich B M 1992 *Plasma Sources Sci. Technol*. **1** 36
[36] Phelps A V and Petrovic Z L 1999 *Plasma Sources Sci. Technol*. **8** R21
[37] Ali M A and Stone P M 2008 *Int. J. Mass Spectrom*. **271** 51
[38] Deutsch H *et al* 2004 *Int. J. Mass Spectrom*. **233** 39
[39] Kolokolov N B and Blagoev A B 1993 *Phys.-Usp*. **36** 152
[40] Lymberopoulos D P and Economou D J 1993 *J. Appl. Phys.* **73** 3668
[41] Thorsteinsson E G and Gudmundsson J T 2010 *J. Phys. D: Appl. Phys.* **43** 115201
[42] Denysenko I B, Kersten H and Azarenkov N A 2015 *Phys. Rev. E* **92** 033102
[43] Maresca A, Orlov K and Kortshagen U 2002 *Phys. Rev.* E **65** 056405
[44] Mityureva A A and Smirnov V V 2004 *Opt. Spektrosk*. **97** 508
[45] Denysenko I, Yu M Y, Ostrikov K and Smolyakov A 2004 *Phys. Rev. E* **70** 046403
[46] Yanguas-Gil A, Cotrino J and Alves L 2005 *J. Phys. D: Appl. Phys*. **38** 1588
[47] Bogaerts A, Gijbels R and Vlèek J 1998 *J. Appl. Phys.* **84** 121
[48] Khrapak S A *et al* 2005 *Phys. Rev. E* **72** 016406
[49] Byrne G D and Thompson S 2013 *VODE_F90 Support Page*, http: //www.radford.edu/~thompson/vodef90web
[50] Sadeghi N 2004 *J. Plasma Fusion Res.* **80** 767
[51] Sikimić B, Stefanović I, Denysenko I B and Winter J 2013 *Plasma Sources Sci. Technol.* **22** 045009
[52] Despiau-Pujo E, Brihoum M, Bodart P, Darnon M and Cunge G 2014 *J. Phys. D. Appl. Phys.* **47** 455201
[53] Lieberman M A and Ashida S 1996 *Plasma Sources Sci. Technol.* **5** 145
[54] Carbone E, Sadeghi N, Vos E, Hübner S, van Veldhuizen E, van Dijk J, Nijdam S and Kroesen G 2015 *Plasma Sources Sci. Technol.* **24** 015015
[55] Gudmundsson J T 2001 *Plasma Sources Sci. Technol.* **10** 76
[56] Mikikian M *et al* 2003 *New J. Phys*. **5** 19
[57] Khrapak S A and Morfill G E 2012 *Phys. Plasmas* **19** 024510